Analysis of Force Shape Characteristics and Detection of Depth-of-Cut Variations in End Milling

Liuqing Yang

Richard E. DeVor

Shiv G. Kapoor

Department of Mechanical and Industrial Engineering,
University of Illinois at Urbana-Champaign,
Urbana, IL 61801

This paper proposes an analytical approach to detect depth-of-cut variations based on the cutting-force shape characteristics in end milling. Cutting forces of a single-flute end mill are analyzed and classified into three types according to their shape characteristics. Cutting forces of a multiple-flute end mill are then classified by considering both the cutting types of the corresponding single-flute end mill and the degree of overlap of successive flutes in the cut. Force indices are extracted from the cutting forces and depth-of-cut variations are detected based on the changes of the force shape characteristics via the force indices in an end-milling process. The detection methodology is validated through cutting experiments. [DOI: 10.1115/1.1947207]

1 Introduction

As an established technology, process monitoring provides significant economic benefits in a wide range of applications, including quality and productivity improvements. It is claimed that the application of monitoring systems to machine tools in production plants has improved the effective cutting time by 10–65% [1]. A basic premise of force-based process monitoring systems is that the cutting force under process faults, such as tool breakage and excessive tool wear, will be significantly higher than the cutting force in fault-free situations. Therefore, threshold values can be prescribed for the process monitoring system to detect process faults [2–5]. However, process variations, such as depth-of-cut (DOC) variation due to part stock variations, can cause changes in the cutting-force signal that lead to violation of the prescribed threshold values and is a major cause of false alarms in such commercial process-monitoring systems whose primary purpose is to detect tool chipping, breakage, and tool wear. In order to avoid those false alarms by adaptively adjusting the thresholds according to the process variations in the monitoring systems, it is necessary to develop methods that can identify both the nature and magnitude of the process variations, independent of process faults, in the multiple-fault environment of process monitoring. Furthermore, such knowledge of process variations can lead to better control of the quality of the product.

Although in the past 15–20 years, researchers have developed many new techniques, such as frequency- and wavelet-based methods that have greatly improved the old threshold-based method, the majority of the machine tool condition-monitoring systems used today still work on more simple principles, including force- and power-based monitoring systems employing threshold values [6]. The methodology proposed herein was specifically designed with this idea in mind. The use of these monitoring systems has been greatly encumbered by false alarms because of the presence of the increase of cutting force due to the phenomenon of DOC variations. The goal of this paper is to find a method that can uniquely distinguish DOC variations.

In any given end-milling application, axial and/or radial depth of cut will vary from the nominal-programmed value due to small part-to-part variations in the amount of stock on the piece or part, its placement and/or positioning in the fixture, system deflections, etc. Variations within some range would be considered normal, and we would not wish our monitoring system to detect them as "important." However, at some point, depth-of-cut variations could be large enough to suggest that a change(s) has (have) occurred that we would want to know about, e.g., core shifts in a casting mold, movement of a fixture locator, and/or part misalignment. Although the limits of normal variations will vary from one situation to another, it may not be unreasonable to think of variations within a few percent (perhaps under 10%) not worthy of detection and most likely will not lead to false alarm in the monitoring system. Conversely, we would like our monitoring system to be able to detect larger variations with high probability. It is an objective of this research to develop an on-line depth-of-cut variation scheme that would be able to estimate DOC variations in the range of 10–50% or greater with errors of no larger than 10–15%, on average.

Several researchers have proposed methods for the estimation of cutting depths in end milling. Altintas and Yellowly [2,7] evaluated the axial and radial depths of cut by fitting polynomial formulas using the ratio of two orthogonal forces measured from a machine spindle. This method required calibration of each tool-workpiece combination and the results were limited to the straight cutting-edge cases (i.e., zero helix angle). Choi and Yang [8] proposed an analytical algorithm for calculating the cutting depths based only on the shape of the cutting-force patterns. However, the method fails to correctly estimate the depths of cut when the radial depth of cut is approaching the cutter diameter. Yang et al. [9] proposed a methodology to estimate the actual depths of cut on-line and hence adaptively adjust the force threshold in a monitoring system. Their results are limited to single-tooth immersion cases. In [10], Yang et al. proposed a model-based methodology and utilized wavelet and force indices to detect DOC variations. However, the wavelet analysis approach requires the building of a large database, and the resolution of the methodology deteriorates when the radial depth of cut increases.

The purpose of this paper is to develop a comprehensive methodology to detect variations in the axial and radial depths of cut in end milling. The methodology should be sensitive to variations in cutting depths, while at the same time not dependent on factors such as part-to-part changes in hardness, cutting speed, feed, and runout. In [8–10], it has been pointed out that both the force magnitude and force shape characteristics will be affected by the DOC variations. Although force magnitude is sensitive to cutting

Contributed by the Manufacturing Engineering Division for publication in the ASME JOURNAL OF MANUFACTURING SCIENCE AND ENGINEERING. Manuscript received July 10, 2003; final revision received August 6, 2004. Associate Editor: C. J. Li.

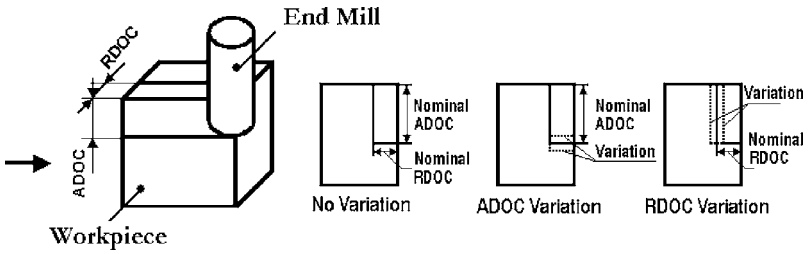

Fig. 1 ADOC and RDOC variations in end milling

conditions (feed rate, speed and depths of cut, etc.) and faults, force shape characteristics are mainly affected by the depths of cut for an end mill with a given number of flutes and helix angle. Therefore, it is possible to find a methodology to detect the DOC variations through the force shape characteristics. In this paper, cutting forces are classified into three fundamental types according to their shape characteristics. Force indices are defined, and characteristic equations are derived to relate DOC variations and force shape characteristics of each type. The methodology is validated through cutting experiments.

2 Theory Behind Detection of DOC Variations Using Force Characteristics Analysis

2.1 Definition of DOC Variations. DOC variations in an end-milling process are characterized by the changes in the nominal (programed) axial depth of cut (ADOC) and/or radial depth of cut (RDOC), as shown in Fig. 1. Hereafter, ADOC and RDOC variations will be denoted as δADOC and δRDOC, respectively. The δADOC and δRDOC are calculated as follows:

$$\delta\text{ADOC} = \frac{\text{ADOC} - \text{ADOC}^{\text{Nom}}}{\text{ADOC}^{\text{Nom}}}$$
$$\delta\text{RDOC} = \frac{\text{RDOC} - \text{RDOC}^{\text{Nom}}}{\text{RDOC}^{\text{Nom}}} \tag{1}$$

where ADOC and RDOC are the actual ADOC and RDOC, ADOC^{Nom} and RDOC^{Nom} are the nominal ADOC and RDOC, respectively.

2.2 Classification of End-Milling Forces.

2.2.1 Single-Flute End Mill. For a single-flute end mill, Sabberwal and Koenigsberger [11] and Tlusty and MacNeil [12] have analyzed the cutting forces of the up-milling case. In their studies, the cutting forces are classified into two types according to relative magnitudes of the cutter engagement angle α_{en} and cutter sweep angle α_{sw} as shown in Fig. 2. If $\alpha_{\text{en}} \geq \alpha_{\text{sw}}$, the force is considered to be type I and if $\alpha_{\text{en}} < \alpha_{\text{sw}}$, the force is considered to be type II. However, their classifications are incomplete because they neglected to include a third type of cutting, heretofore referred to as type III, that occurs only if $\text{RDOC} \geq R$, where R is the cutter radius.

A typical resultant force profile (F_r) generated by a single-flute end mill is shown in Fig. 3 as a function of the angular engagement (θ). There are three characteristic points in the force profile: entry point (θ_1), peak point (θ_2), and exit point (θ_3). For milling using a single-flute end mill with a given helix angle, the locations of and distances between these characteristic points are determined by the depths of cut. To obtain the relationship between the force shape characteristics and depths of cut, the formation of the cutting force for a single-flute end milling must be studied via cutter-workpiece engagement analysis.

We define the cutter-workpiece engagement section in Figs. 4(*a*) and 4(*b*), as a rectangle denoted as *abcd*. The edge *ab* is the entry edge where the flute starts to cut. The length of *ab* is equal to ADOC. The edge *bc* is the top edge such that the part of the flute above this edge will not be engaged in cutting. The length of *bc* equals $R\alpha_{\text{en}}$. The edge *cd* is the exit edge where the flute exits from the workpiece. The edge *da* is the bottom edge where the bottom of the cutter meets the workpiece for a step cut, as defined in Figs. 4(*a*) and 4(*b*). Vertex *a* is the entry point, and vertex *c* is the exit point, as defined in Fig. 3. The instantaneous chip thickness can be obtained from hatched arc in the top of Fig. 4(*b*), where t_c is the uncut chip thickness.

To classify the cutting forces according to their shape characteristics, two critical values, ADOC_c and $\text{RDOC}_c(\alpha_{\text{enc}})$, are defined. ADOC_c is defined as the ADOC where α_{sw} equals α_{en}. Vertex b' is a corresponding point of vertex *b* when ADOC equals ADOC_c. ADOC_c can be calculated using the following:

$$\text{ADOC}_c = \frac{R\alpha_{\text{en}}}{\tan\alpha_{hx}} = \frac{R\cos^{-1}\left(1 - \dfrac{\text{RDOC}}{R}\right)}{\tan\alpha_{hx}} \tag{2}$$

where α_{hx} is the helix angle of the end mill. RDOC_c is defined as the RDOC where the half-immersion line (in Fig. 4(*b*)) goes through the center of the engaged flute. Vertex b'' is a corresponding point of vertex *b* when $\text{RDOC} = \text{RDOC}_c$. RDOC_c can be calculated using the following:

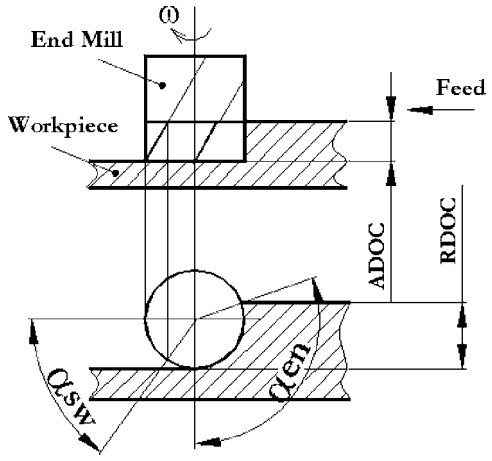

Fig. 2 Cutter engagement angle α_{en} and cutter sweep angle α_{sw}

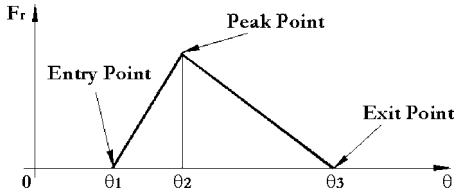

Fig. 3 Typical force profile for single-flute end milling

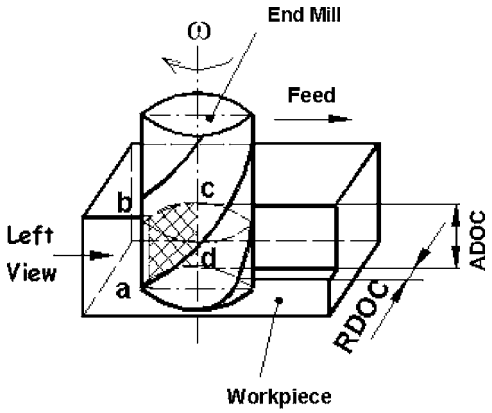

(a) End Milling Process

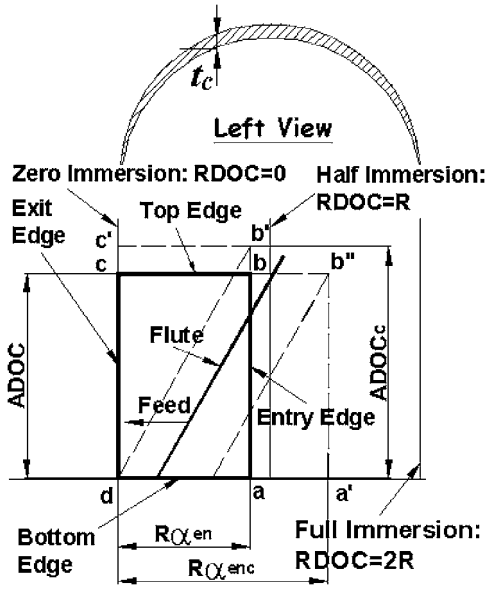

(b) Expanded Engagement Section

Fig. 4 Cutter-workpiece engagement section

$$\alpha_{enc} = \frac{\pi + \alpha_{sw}}{2}, \qquad \mathrm{RDOC}_c = R(1 - \cos\alpha_{enc}) = R\left[1 + \sin\left(\frac{\mathrm{ADOC}_c \tan\alpha_{hx}}{2R}\right)\right] \tag{3}$$

The classification of the cutting force for single-flute end milling is done by comparing the actual depths of cut to ADOC_c and RDOC_c.

Type-I Cutting: $\mathrm{RDOC} < \mathrm{RDOC}_c$ *and* $\mathrm{ADOC} < \mathrm{ADOC}_c$. As shown in Fig. 5(*a*), when the flute moves from *a* to *b*, the cutting force increases because the engaged length of flute increases continuously. When the flute moves from *b* to *d*, the engaged length of the flute is constant, but cutting force decreases because the chip thickness t_c decreases. When the flute moves from *d* to *c*, the cutting force decreases because the engaged length of the flute decreases continuously until the cutter is completely out of the cut. Therefore, the peak point occurs at *b*. The angular distance between the entry point and peak point is α_{sw} and the distance between the exit and peak points is α_{en}. Figure 5(*b*) shows the force profile generated during the type-I cutting.

Type-II Cutting: $\mathrm{RDOC} < \mathrm{RDOC}_c$ *and* $\mathrm{ADOC} \geqslant \mathrm{ADOC}_c$. As shown in Fig. 6(*a*), when the flute moves from *a* to *d*, the cutting force increases because the engaged length of flute increases. When the flute moves from *d* to *b*, the engaged length of the flute is constant. The cutting force is constant because the chip load is constant. When the flute moves from *b* to *c*, the cutting force decreases because the engaged length of the flute decreases continuously until the cutter is completely out of the cut. Therefore, the peak point occurs at vertex *d*. From vertex *d* to *b*, there is a flat top. The angular distance between the entry and peak points is α_{en} and the distance between the exit and peak points is α_{sw}. Figure 6(*b*) shows the force profile generated during the type-II cutting.

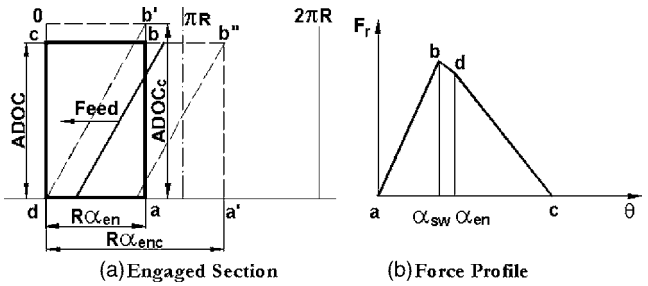

Fig. 5 Type-I cutting for single-flute end milling

Type-III Cutting: $\mathrm{RDOC} \geqslant \mathrm{RDOC}_c$ *and* $\mathrm{ADOC} < \mathrm{ADOC}_c$. As shown in Fig. 7(*a*), when the flute moves from *a* to *b*, the cutting force increases because the engaged length of flute increases continuously. When the flute moves from *b* to *b*″, the engaged length of the flute is constant. However, the cutting force still increases because the chip thickness increases. When the flute moves from *b*″ to *d*, the engaged length of the flute is still constant. However, the cutting force decreases because the chip thickness decreases. When the flute moves from *d* to *c*, the cutting force decreases because the engaged length of the flute decreases continuously until the cutter is completely out of the cut. Therefore, the peak point occurs at *b*″. The angular distance between the entry and

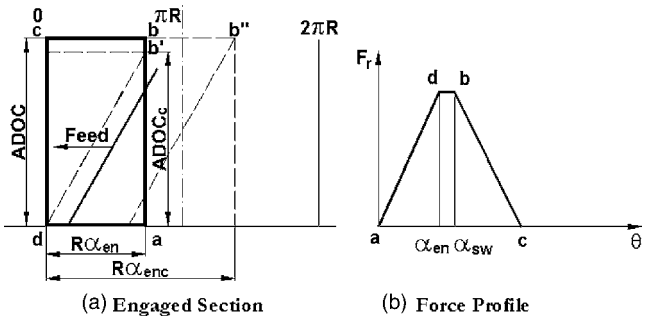

Fig. 6 Type-II cutting for single-flute end milling

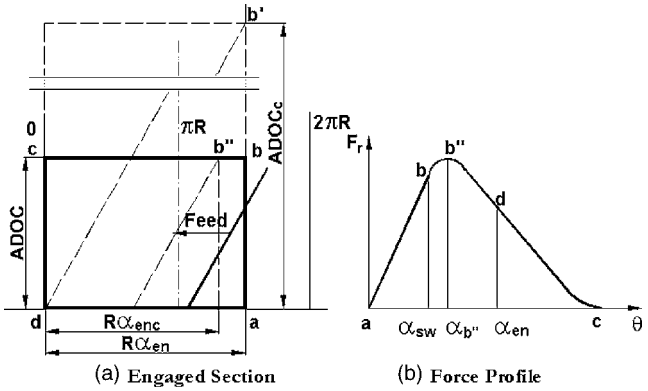

Fig. 7 Type-III cutting for single-flute end milling

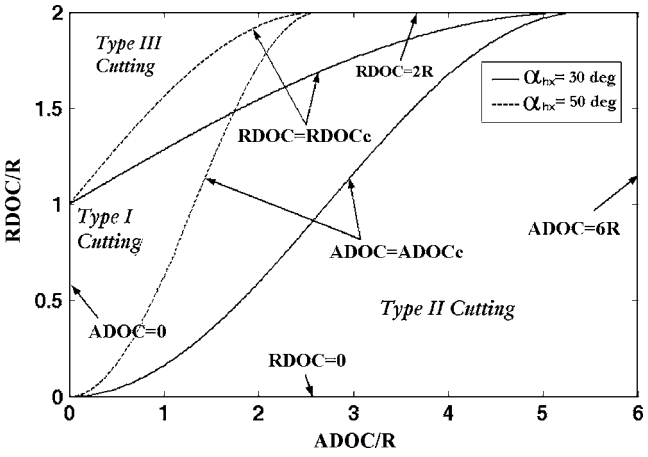

Fig. 8 Classification of cutting types for single-flute end milling

peak points is $\alpha_{b''}=\alpha_{sw}+\alpha_{en}-\alpha_{enc}$ and the distance between the exit and peak points is α_{enc}. Figure 7(*b*) shows the force profile generated during the type-III cutting. Note that according to the definition of $ADOC_C$ and $RDOC_C$ in Eqs. (2) and (3), cutting with $RDOC \geqslant RDOC_c$ and $ADOC \geqslant ADOC_c$ cannot occur.

A graphical representation of the classification of the three cutting types as a function of the axial and radial depths of cut is shown as Fig. 8 where the range of RDOC is [0, 2R] and the range of ADOC is [0, 6R]. The solid and dashed lines are the cutting types for an end mill with $\alpha_{hx}=30$ deg and with $\alpha_{hx}=50$ deg, respectively. It is seen from Fig. 8 that when the helix angle increases, type-I and -III regions shrink, whereas type-II region increases. It is clear from Fig. 8 that for $ADOC/R>6$, the cutting will always be type II for these two helix angles.

It should be pointed out that although all the above analysis and conclusions were made with down-milling, the classification is valid for up-milling as well. In Fig. 4, if the feed direction is reversed, the cutting becomes up-milling. The cutter-workpiece engagement section *abcd* (defined in Fig. 4) is the same. However, vertex *c* becomes the entry point, edge *cd* becomes the entry edge, vertex *a* becomes the exit point, and edge *ab* becomes the exit edge. The classification of cutting forces in up-milling is the same as in down-milling, as given by Eqs. (2) and (3).

2.2.2 Multiple-Flute End Mill. Since the cutting forces of a multiple-flute end mill are the sum of the forces of the corresponding single-flute end mill, the shape characteristics of the cutting force for a multiple-flute end mill will depend on those of the single-flute end mill. In addition, the cutting forces for a multiple-flute end mill will have their own characteristics because the immersion type will change according to the depths of cut and tool geometry.

For an end-milling process, there are two types of immersion—single-tooth immersion (STI) and multiple-tooth immersion (MTI). As shown in Fig. 9, if the flute engagement angle β is less than the flute spacing angle α_T (which equals $2\pi/N_f$, where N_f is the number of flutes), the cutter is in STI; otherwise, it is in MTI.

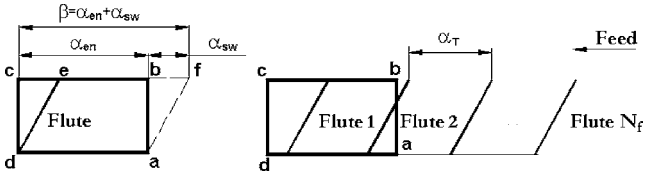

Fig. 9 Flute engagement in end milling

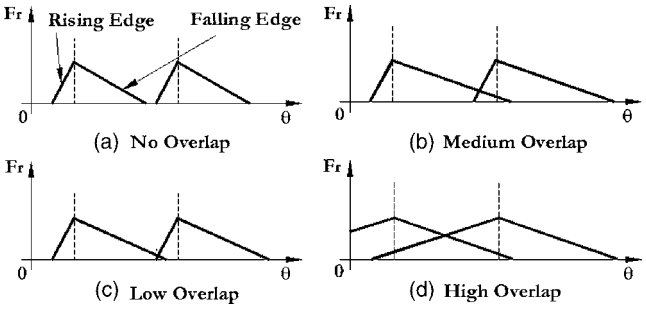

Fig. 10 Classification of flute overlap

Equation (4) is the generalized formula for determining the maximum number of flutes engaged in cutting for a given cutter and given cutting conditions:

$$n=\lceil \beta/\alpha_T \rceil, \tag{4}$$

where n is the number of flutes engaged in cutting and $\lceil \beta/\alpha_T \rceil$ denotes to round β/α_T to the nearest integer toward infinity. If $n=1$, the cutter is in STI; and if $n>1$, the cutter is in MTI.

The shape characteristics of the cutting force of a multiple-flute end mill can be determined by considering both the characteristics of the corresponding single-flute end mill and the immersion type. The immersion type in MTI may be further classified according to the degree of overlap (DOO). In Fig. 10, the DOO is classified into four categories: no overlap (NO), low overlap (LO), medium overlap (MO), and high overlap (HO). When there is no overlap (Fig. 10(*a*)), the cutter is in STI. Low overlap (Fig. 10(*b*)) occurs when the rising edge of a flute force overlaps with the falling edge of the preceding flute force. Medium overlap (Fig. 10(*c*)) occurs when both the rising and falling edges of a flute force overlap with the falling edge of the preceding flute force, but the rising edge does not overlap with the rising edge of the preceding flute force. High overlap (Fig. 10(*d*)) occurs when the rising edge of a flute force overlaps with the rising edge of the preceding flute force.

There will be a total of 12 (3 cutting types multiply 4 degrees of overlap) different shape characteristics (categories) for the cutting forces of a multiple-flute end mill. An example of the classification is shown graphically in Fig. 11 for an end mill with three flutes and a helix angle of 30 deg. There are three dashed lines in Fig. 11. They are $\alpha_{en}+\alpha_{sw}=\alpha_T$, $\alpha_{en}=\alpha_T$, and $\alpha_{sw}=\alpha_T$ which are determined by the definition of different degrees of overlap. It can be inferred from Fig. 11 that NO and LO will be the most common cutting types, whereas HO will be very unlikely to occur for this end mill.

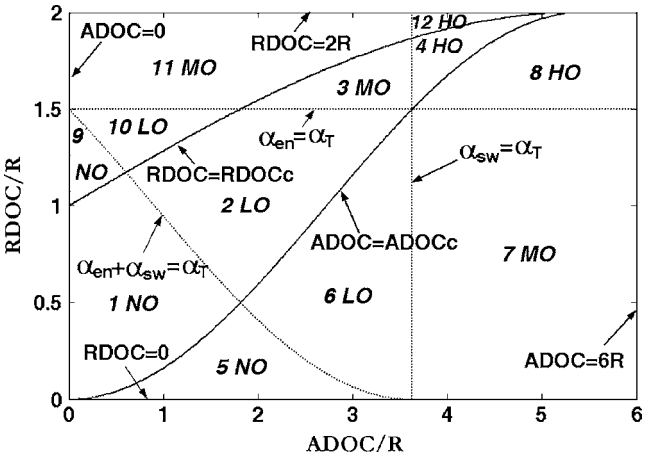

Fig. 11 Classification of cutting types for multiple-flute end milling

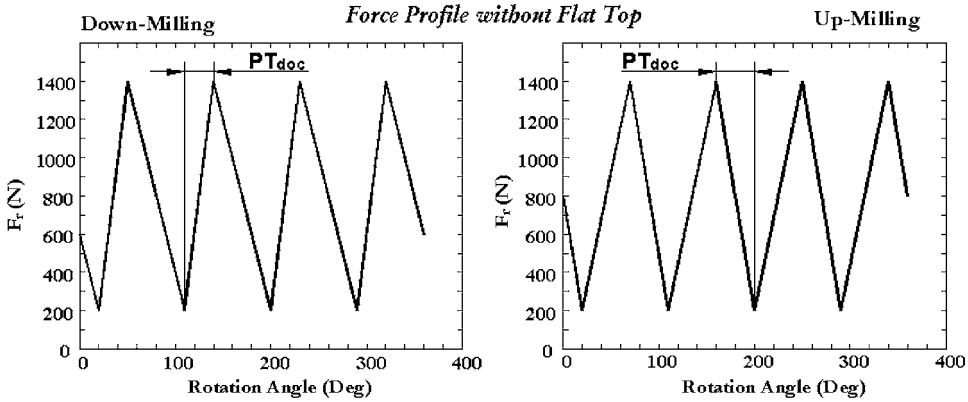

(a) Force Index for Force Profile without Flat Top

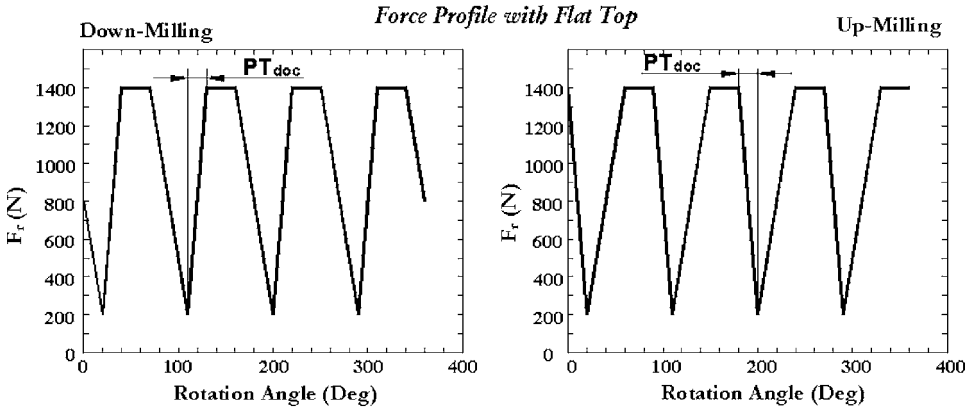

(b) Force Index for Force Profile with Flat Top

Fig. 12 Definition of force index PT_{doc}

2.3 Definition and Analysis of Force Indices. To quantify the effects of DOC variations on force shape characteristics and therefore detect the DOC variations, two force indices are defined (as shown in Fig. 12) to reflect the shape characteristic changes with respect to DOC variations. One of the force indices is PT_{doc}, which is defined as the angular distance between the force valley and force peak immediately following it (for up-milling, it is defined as the angular distance between the force peak and force valley immediately following it). For a cutting force without a flat top, the force index PT_{doc} is defined as in Fig. 12(*a*); otherwise, it is defined as in Fig. 12(*b*). This force index reflects one of the important shape characteristics of the cutting forces in the angular dimension. Another force index PT_{ave} is defined as the average force over one revolution.

As we know from Sec. 2.2.2, the cutting forces for a multiple-flute end mill are classified into 12 categories. We will quantify the relationship between the force index PT_{doc} and depth of cut for each category in the following paragraphs.

2.3.1 Type I Cutting. Figure 13(*a*)–13(*d*) shows four possible categories of the cutting forces for a multiple-flute end mill whose corresponding single-flute end mill is engaged in type-I cutting. The relationship between the force index PT_{doc} and the characteristic angles is

$$PT_{doc} = \begin{cases} \alpha_{sw}, & \text{if } \alpha_{sw} < \alpha_T \\ \alpha_{sw} - n\alpha_T & \text{if } \alpha_{sw} \geqslant n\alpha_T, n = 1,2,\cdots,N_f - 1 \end{cases} \quad (5)$$

Accordingly, for categories 1–3, the force index PT_{doc} equals α_{sw}, and for category 4, the force index PT_{doc} equals α_{sw}-$n\alpha_T$.

2.3.2 Type-II Cutting. Figure 14(*a*)–14(*d*) show four possible force categories of the cutting forces for a multiple-flute end mill whose corresponding single-flute end mill is engaged in type-II cutting. The relationship between the force index PT_{doc} and the characteristic angles is:

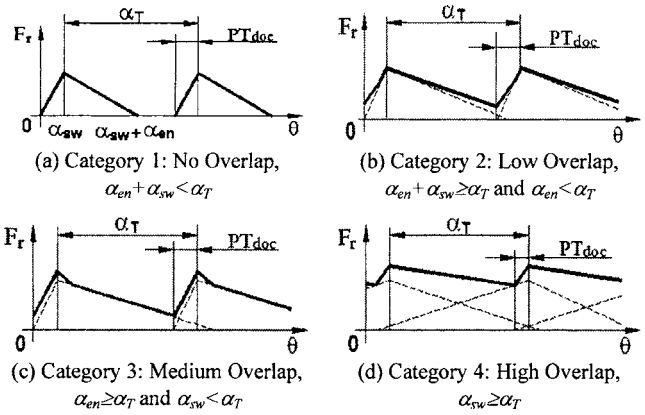

(a) Category 1: No Overlap, $\alpha_{en}+\alpha_{sw}<\alpha_T$

(b) Category 2: Low Overlap, $\alpha_{en}+\alpha_{sw}\geq\alpha_T$ and $\alpha_{en}<\alpha_T$

(c) Category 3: Medium Overlap, $\alpha_{en}\geq\alpha_T$ and $\alpha_{sw}<\alpha_T$

(d) Category 4: High Overlap, $\alpha_{sw}\geq\alpha_T$

Fig. 13 Force profiles of type-I cutting in MTI

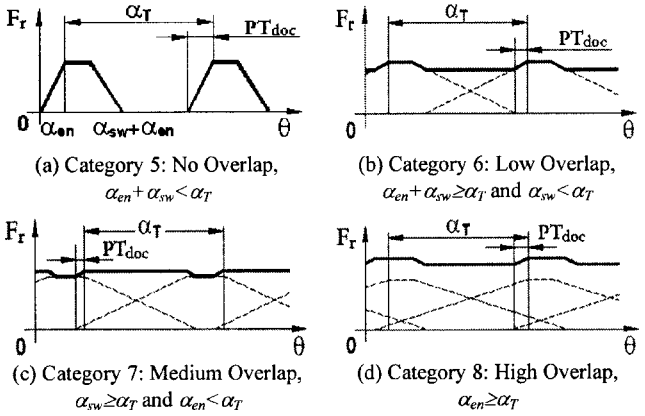

Fig. 14 Force profiles of type-II cutting in MTI

$$PT_{doc} = \begin{cases} \alpha_{en} & \text{if } \alpha_{sw} < \alpha_T \\ \alpha_T - \alpha_{sw} & \text{if } \alpha_{sw} < \alpha_T \text{ and } \alpha_{en} + \alpha_{sw} \geqslant \alpha_T \\ \alpha_{sw} - \alpha_T, & \text{if } \alpha_{en} < \alpha_T \text{ and } \alpha_{sw} \geqslant \alpha_T \\ \alpha_{en} - n\alpha_T, & \text{if } \alpha_{en} \geqslant n\alpha_T, n = 1,2,\cdots,N_f - 1 \end{cases} \quad (6)$$

Accordingly, for categories 5, the force index $PT_{doc}=\alpha_{en}$. For category 6, $PT_{doc}=\alpha_T-\alpha_{sw}$. For category 7, $PT_{doc}=\alpha_{sw}-\alpha_T$, and for category 8, $PT_{doc}=\alpha_{en}-n\alpha_T$.

2.3.3 Type-III Cutting. Figure 15(*a*)–15(*d*) shows four possible force categories of the cutting forces for a multiple-flute end mill whose corresponding single-flute end mill is engaged in type-III cutting. The relationship between the force index PT_{doc} and the characteristic angles is

$$PT_{doc} = \begin{cases} \alpha_{en} + 1/2 \cdot (\alpha_{sw} - \pi), & \text{if } \alpha_{enc} \geqslant \alpha_T \\ & \text{and } \alpha_{sw} + (\alpha_{en} - \alpha_{enc}) < \alpha_T \\ \alpha_{en} + 1/2 \cdot (\alpha_{sw} - \pi) - n\alpha_T, & \text{if } \alpha_{sw} + (\alpha_{en} - \alpha_{enc}) \\ & \geqslant n\alpha_T, n = 1,2,\ldots,N_f - 1 \end{cases} \quad (7)$$

Accordingly, for all categories 9–11, the force index $PT_{doc}=\alpha_{en}+1/2^{*}(\alpha_{sw}-\pi)$. For category 12, the force index $PT_{doc}=\alpha_{en}+1/2^{*}(\alpha_{sw}-\pi)-n\alpha_T$.

Therefore, the relationship between the force PT_{doc} index and the cutting angles are described by characteristic Eqs. (5)–(7) and

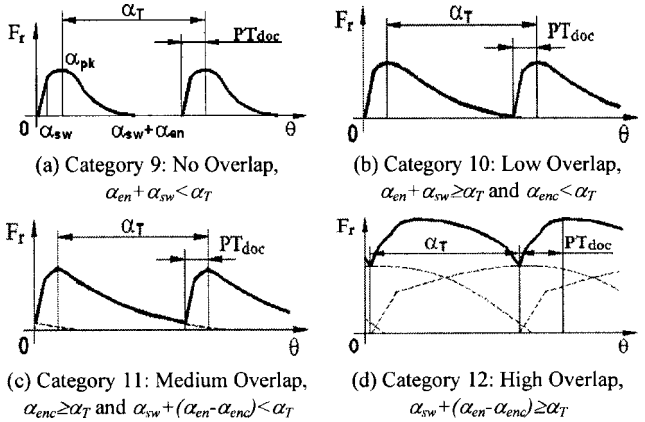

Fig. 15 Force profiles of type-III cutting in MTI

Table 1 Summary of the Calculation of PT_{doc}

	NO	LO	MO	HO
Type I	α_{en}	α_{sw}	$\alpha_{sw}-\alpha_T$	$\alpha_{sw}-n\alpha_T$
Type II		$\alpha_T-\alpha_{sw}$		$\alpha_{en}-n\alpha_T$
Type III		$\alpha_{en}+\frac{1}{2}(\alpha_{sw}-\pi)$		$\alpha_{en}+\frac{1}{2}(\alpha_{sw}-\pi)-n\alpha_T$

are summarized in Table 1. Furthermore, the relationship between the cutting angles and depths of cut can be obtained using the following equation:

$$\text{ADOC} = \frac{\alpha_{sw} \cdot R}{\tan \alpha_{hx}}$$
$$\text{RDOC} = R(1 - \cos \alpha_{en}) \quad (8)$$

The relationship between the force index PT_{ave} and depths of cut can be approximated using the following rigid average force model [3]:

$$PT_{ave} = K \cdot \text{ADOC} \cdot \text{RDOC}, \quad (9)$$

where K is the specific cutting energy.

Therefore, relationships between the force indices and depths of cut are established with Eqs. (5)–(9).

2.4 Estimation of DOC Variations via Force Indices. In a cutting practice, the actual cutting-force signal is obtained through the force-monitoring system. Force indices PT_{doc} and PT_{ave} may be extracted from the actual cutting force. To estimate the DOC variations using the force indices PT_{doc} and PT_{ave}, we need to choose the correct characteristic equation from Table 1, depending on the actual cutting type and degree of overlap (DOO). However, since the actual depths of cut are unknown, the actual cutting type and DOO are unknown.

A simple approach to solve this dilemma is to substitute the force indices PT_{doc} and PT_{ave} into all the characteristic equations and solve for all possible combinations of depths of cut, then compare the results to the nominal depths of cut and eliminate those that fall well away from the nominal value, say beyond ±50%. The values left after this elimination process will be the estimated DOC variations and the associated cutting type and DOO. If there are more than one combination of DOC variations available, we should conduct another check by calculating the cutting type using Eqs. (2) and (3) and the DOO, referring to Fig. 10 with the estimated depths of cut and comparing them to the associated cutting type and DOO. If the two cutting types and DOOs agree, the associated DOC variations are correct. If these estimated DOC variations are within ±10% of the nominal, we will assume they are "normal," as discussed earlier, and no fault of this nature is detected.

3 Experimental Validation

The detection of DOC variations from one part to another is an important problem from several standpoints, including both process performance and part quality issues. As such, it is a low-frequency phenomenon. In fact, within a part, where the force

Table 2 Cutting parameters

Cutting parameters	End mill 1	End mill 2
Tool material	PVD Coated	TICN Coated
Number of flutes	4	3
Helix angle (deg)	30	50
End-mill diameter (mm)	19.05	9.525
Radial rake angle (deg)	3	6
Feed rate (mm/tooth)	0.0381	0.0254

Table 3 Nominal depths of cut

Cutting type	End mill 1 (mm)		End mill 2 (mm)	
	$ADOC^{Nom}$	$RDOC^{Nom}$	$ADOC^{Nom}$	$RDOC^{Nom}$
I	7.62	7.62	3.81	3.81
II	20.32	2.54	10.16	1.27
III	2.54	15.24	1.27	7.62

signature is to be evaluated online, its frequency of occurrence may be assumed zero. In this validation, the experiments were designed specifically with this in mind.

In order to detect the DOC variations using the force indices, the continuous time cutting-force signal obtained from the force sensor needs to be sampled or digitalized into discrete time series. Usually, the sampling rate is determined by the Rule of Nyquist. However, in this study, the sampling rate of the A/D conversion must be much higher than the Nyquist frequency for the discrete force signal to have adequate angular resolution to reflect the small amount of angular variations incurred by the depth-of-cut variations. These small angular variations are $\delta\alpha_{sw}$ and $\delta\alpha_{en}$, which are given by

$$\delta\alpha_{sw} = \frac{\delta\text{ADOC} \cdot \text{ADOC}^{\text{Nom}}}{R} \tan \alpha_{hx}, \tag{10}$$

$$\delta\alpha_{en} = \cos^{-1}\left(1 - \frac{\text{RDOC}^{\text{Nom}}(1+\delta\text{RDOC})}{R}\right) - \cos^{-1}\left(1 - \frac{\text{RDOC}^{\text{Nom}}}{R}\right) \tag{11}$$

For a small quantity, such as δRDOC, Eq. (11) can be expanded using Taylor series. The resulting equation is

$$\delta\alpha_{en} = \frac{\delta\text{RDOC} \cdot \text{RDOC}^{\text{Nom}}}{R\sqrt{2\left(\frac{\text{RDOC}^{\text{Nom}}}{R}\right) - \left(\frac{\text{RDOC}^{\text{Nom}}}{R}\right)^2}}. \tag{12}$$

In this methodology, $\delta\alpha_{sw}$ and $\delta\alpha_{en}$ will reach their respective minimum values when the δADOC and δRDOC equal to the resolution (the smallest unit of DOC variations we can differentiate) of the detection of DOC variations, i.e., b. Therefore, the sampling rate (measured in points/rev) must satisfy the following criterion:

Table 4 DOC Variations Test Conditions for Each Cutting Type

Test No.	End mill 1 (%)		End mill 2 (%)	
	δADOC	δRDOC	δADOC	δRDOC
1	−20	0	0	20
2	20	5	−5	−20
3	−20	10	−10	20
4	20	15	−15	−20
5	−20	20	−20	20

$$\text{Sampling Rate} > \text{Max}\left(\frac{2\pi R}{b \cdot \text{ADOC}^{\text{Nom}} \cdot \tan \alpha_{hx}} \times \frac{2\pi R\sqrt{2\frac{\text{RDOC}^{\text{Nom}}}{R} - \left(\frac{\text{RDOC}^{\text{Nom}}}{R}\right)^2}}{b \cdot \text{RDOC}^{\text{Nom}}}\right) \tag{13}$$

For example, for an end mill with three flutes and a helix angle of 30 deg, with $ADOC^{Nom}$=10 mm, $RDOC^{Nom}$=10 mm, and spindle speed=1000 rpm, assuming the resolution of the detection b =1%, the sampling rate determined by Eq. (13) should be max (1,021,587)=1021 points/rev=17,017 Hz. The sampling rate given by the Nyquist Rule is 100 Hz.

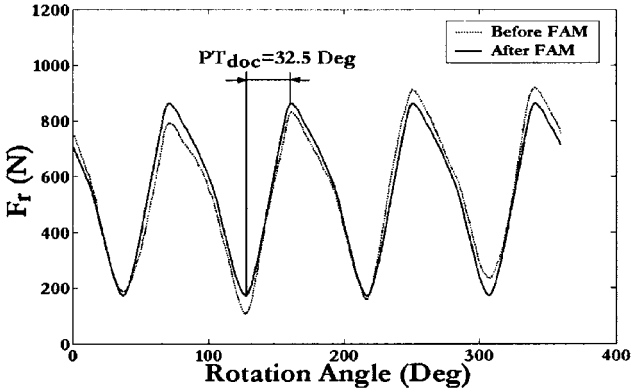

(a) Cutting Type I, Cutter#1 and Test#4 in Table 5

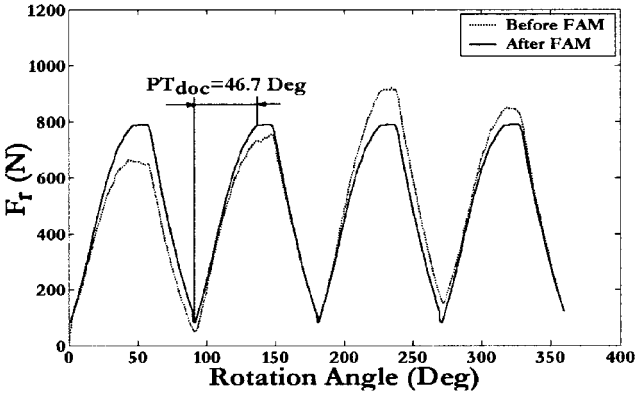

(b) Cutting Type II, Cutter#1 and Test#5 in Table 6

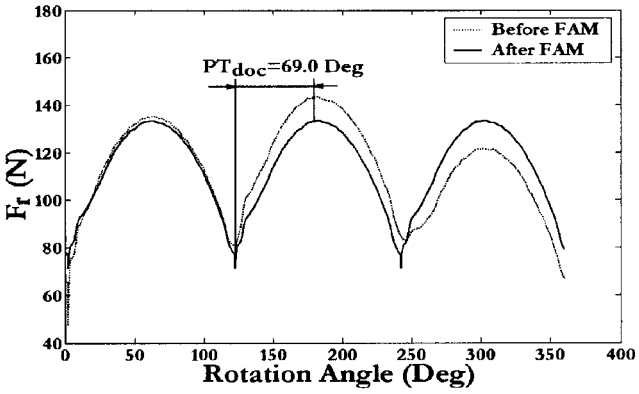

(c) Cutting Type III, Cutter#2 and Test#4 in Table 7

Fig. 16 Examples showing the extraction of force index PT_{doc}

Table 5 Estimated DOC variations for Cutting Type I

Test No.	δADOC (%)	Abs. Est. Err. of δADOC (%)	Rel. Est. Err. of δADOC (%)	δRDOC (%)	Abs. Est. Err. of δRDOC (%)	Rel. Est. Err. of δRDOC (%)
			(a) End mill 1			
1	−18.14	1.86	−9.31	−2.40	−2.4	N/A
2	17.86	−2.14	−10.71	6.22	1.22	24.33
3	−17.46	2.54	−12.69	8.24	−1.76	−17.62
4	22.72	2.72	13.59	12.64	−2.36	−15.74
5	−17.13	2.87	−14.37	18.16	−1.84	−9.19
			(b) End mill 2			
1	2.44	2.44	N/A	18.36	−1.64	−8.21
2	−2.65	2.35	−46.93	−22.52	−2.52	12.59
3	−7.98	2.02	−20.24	17.17	−2.83	−14.14
4	−16.11	−1.11	7.38	−18.78	1.22	−6.08
5	−17.66	2.34	−11.71	17.00	−3.00	−15.00

To validate the methodology, down-milling tests using two right-handed helical end mills with different geometries and coating as shown in Table 2 were performed on a MORI SEIKI SV503 Vertical Machining Center. The workpiece material used was 1018 steel. The nominal depths of cut for each cutting type and each end mill are shown in Table 3. The DOC variations test conditions for each cutting type are shown in Table 4, and they remained the same for each cutting type. For each of the experiments, ~20 revolutions of force signals were measured using a Kistler three-axis dynamometer (Type 9265A, the accuracy is ±0.5% of input and the resolution is 0.31 mV). The continuous time force signals from the dynamometer were passed through a Kistler three-channel charge amplifier (Model 5004) and then were filtered using a low-pass filter with a cutoff frequency of 470 Hz to remove the high-frequency noises and transients before sending to the A/D converter. The choice of the cutoff frequency of the low-pass filter is a trade-off between the conservation of information and the elimination of the noise in the raw force signal. The appropriate cutoff frequency may be determined through a residual analysis of the difference between filtered and unfiltered force signals over a wide range of cutoff frequencies [13]. A general relationship between the error of force measurement (and hence the resolution of DOC variation detection) and the cutoff frequency can be found in [14]. Using this relationship, for the resolution of DOC variation detection to be 1%, the cutoff frequency was determined to be seven times of the highest frequency of interest in the cutting-force signal. Therefore, for a four-flute end mill with a spindle speed of 1000 rpm, the cutoff frequency was chosen to be $7\times4\times1000/60\approx470$ Hz. After filtering, the A/D converter digitized or sampled the filtered force signals at a sampling rate of 72 KHz, which yielded 4320 points/rev since the spindle speed is 1000 rpm (the minimum sampling rate is 4081 points/rev according to Eq. (13), assuming $b=1\%$). The discrete time series of the force signal was then sent to a desktop PC. In this study, the resultant force $F_r=\sqrt{F_x^2+F_y^2+F_z^2}$ was used as the force signal for analysis. The flute-average method (FAM) was then applied to the resultant force to remove the effects of runout. In this method, sample points spaced by the flute-spacing angle α_T were averaged over one revolution to obtain an average flute profile.

Examples of the extracting of force index PT_{doc} and the estimating of the DOC variations accordingly are shown in Fig. 16(*a*)–16(*c*) for Types I, II, and III, respectively. The raw resultant cutting forces were obtained through the data acquisition device and then averaged in ten revolutions to remove revolution-to-revolution transients. The FAM method is then applied to the averaged resultant forces to eliminate the effect of runout, as shown in Fig. 16. Considering Fig. 16(*a*) as an example to show how the DOC variations are estimated, we extracted the force indices from the force signal as shown in the Fig. 16(*a*), the values of PT_{doc} and PT_{ave} are directly obtained from F_{FAM} and they were found to be 32.5 deg and 542.2 N, respectively. These values of the PT_{doc} and PT_{ave} were applied in characteristic Eqs. (5)–(9), and solved for all the possible combinations of depths of cut. The only combination having both DOC variations within the specified ±50% range was found to be $[\delta\text{ADOC}=22.72\%, \delta\text{RDOC}=12.64\%]$. For this test condition, the actual δADOC=20% and actual δRDOC

Table 6 Estimated DOC variations for Cutting Type II

Test No.	δADOC (%)	Abs. Est. Err. of δADOC (%)	Rel. Est. Err. of δADOC (%)	δRDOC (%)	Abs. Est. Err. of δRDOC (%)	Rel. Est. Err. of δRDOC (%)
			(a) End mill 1			
1	−17.93	2.07	−10.36	−1.40	−1.4	N/A
2	22.19	2.19	10.95	3.45	−1.55	−31.09
3	−17.13	2.87	−14.33	7.35	−2.65	−26.49
4	18.21	−1.79	−8.95	16.08	1.08	7.19
5	−17.63	2.37	−11.87	17.77	−2.23	−11.17
			(b) End mill 2			
1	0.68	0.68	N/A	17.53	−2.47	−12.34
2	−2.41	2.59	−51.84	−22.34	−2.34	11.71
3	−8.31	1.69	−16.89	18.49	−1.51	−7.54
4	−12.80	2.2	−14.64	−21.84	−1.84	9.20
5	−17.86	2.14	−10.70	18.71	−1.29	−6.44

Table 7 Estimated DOC variations for Cutting Type III

Test No.	δADOC (%)	Abs. Est. Err. of δADOC (%)	Rel. Est. Err. of δADOC (%)	δRDOC (%)	Abs. Est. Err. of δRDOC (%)	Rel. Est. Err. of δRDOC (%)
			(a) End mill 1			
1	−17.45	2.55	−12.77	−2.21	−2.21	N/A
2	23.06	3.06	15.29	2.27	−2.73	−54.79
3	−17.00	3	−14.98	7.51	−2.49	−24.86
4	22.86	2.86	14.28	11.02	−3.98	−26.52
5	−16.12	3.88	−19.42	17.01	−2.99	−14.96
			(b) End mill 2			
1	2.01	2.01	N/A	18.28	−1.72	−8.60
2	−2.25	2.75	−54.95	−22.03	−2.03	10.15
3	−7.06	2.94	−29.39	16.31	−3.69	−18.45
4	−13.40	1.6	−10.65	−22.82	−2.82	14.09
5	−17.23	2.77	−13.84	17.39	−2.61	−13.03

=15%, so the absolute estimation errors are 2.72% and −2.36% and the relative estimation errors, defined as the ratio of the absolute estimation errors and the programed values, are 13.59% and −15.74%, respectively.

The estimation results for all the tests are shown in Tables 5–7 for each cutting type. It can be seen that, although two different end mills with different numbers of flutes, diameter, and helix angle were used in the experiments, the estimated DOC variations, however, showed good consistency. For all the tests, the absolute errors of the estimated DOC variations are <3% on the average. Moreover, for both end mills, when the programed DOC variations are >10%, the relative estimation errors are generally <15%. However, when the programed DOC variations are 10% or smaller, the relative estimation errors incurred are much larger. Hence, it appears that it is possible to achieve our prestated objective of detecting DOC variations of over 10% with estimation errors of 15% or less on the average.

4 Conclusions

This paper has examined the utilization of force indices based on force shape characteristics analysis to detect DOC variations in end milling. The capability of the force indices has been demonstrated through experimentation. Specifically, the following conclusions are reached:

1. The cutting forces of a single-flute end mill may be classified into types I, II, and III, according to their shape characteristics. The cutting forces of a multiple-flute end mill may be further classified into 12 categories (three cutting types multiplied by four degrees of overlap).
2. Force index PT_{doc} is defined as the angular distance between the force valley and force peak immediately following it, and force index PT_{ave} is defined as the average force over one revolution. Characteristic equations are derived to relate the force shape characteristics to the depths of cut via force indices PT_{doc} and PT_{ave}, for each unique cutting-force classification.
3. Based on the experimental data, the utilization of force indices PT_{doc} and PT_{ave} extracted from the cutting forces is shown to detect DOC variations with absolute estimation errors of 3% or less on average.

Acknowledgment

This research has been supported by a grant from the National Science Foundation Center for Machine Tool Systems Research at the University of Illinois.

References

[1] Tonshoff, H. K., Wolfsberg, J. P., Kals, H. J. J., Konig, W., and Luttervelt, C. A., 1988, "Developments and Trends in Monitoring and Control of Machining Process," CIRP Ann., **37**(2), pp. 611–622.

[2] Altintas, Y., and Yellowley, I., 1989, "In-Process Detection of Tool Failure in Milling Using Cutting Force Models," ASME J. Eng. Ind., **111**(2), pp. 149–157.

[3] DeVor, R. E., Kapoor, S. G., Hibner, M., Kim, D., Reutzel, K., and Kline, W. A., 1996, "A Process Model-Based Approach for Machine Tool and Cutting Process Diagnostics," *Proc. of the Japan-USA Symp. on Flexible Automation*, Boston, Massachusetts, pp. 1007–1017.

[4] Dzombak, I., and Kline, W., 1989, "System Design for In-Process Tool Monitors," *SME Technical Paper*, MS89-457.

[5] Tarn, J. H., and Tomizuka, M., 1989, "On-Line Monitoring of Tool and Cutting Conditions in Milling," ASME J. Eng. Ind., **111**(3), pp. 206–212.

[6] Jemielniak, K., 1999, "Commercial Tool Condition Monitoring Systems," Int. J. Adv. Manuf. Technol., **15**, pp. 711–721.

[7] Altintas, Y., and Yellowley, I., 1987, "The Identification of Radial Width and Axial Depth of Cut in Peripheral Milling," Int. J. Mach. Tools Manuf., **27**(3), pp. 367–381.

[8] Choi, J. G., and Yang, M. Y., 1999, "In-Process Prediction of Cutting Depths in End Milling," Int. J. Mach. Tools Manuf., **39**(5), pp. 705–721.

[9] Yang, L. Q., Zhu, R., DeVor, R. E., Kapoor, S. G., and Kline, W. A., 2000, "Identification of Stock Size Variation and its Application to Process Monitoring in End Milling," *Proc. of the Japan-USA Symp. on Flexible Automation*, Ann Arbor, Michigan, Paper No. 2000JUSFA-13212, pp. 1–8.

[10] Yang, L. Q., DeVor, R. E., Kapoor, S. G., 2002, "A Model-Based Methodology for Detection of Depth of Cut Variations in End Milling," *Proc. of the Japan-USA Symp. on Flexible Automation*, Hiroshima, Japan, Vol. 1, Chap. B2, pp. 1–8.

[11] Sabberwal, A. J. P., and Koenigsberger, F., 1960, "Chip Section and Cutting Force During the Milling Operation," CIRP Ann., **9**, pp. 197–203.

[12] Tlusty, J., and MacNeil, P., 1975, "Dynamics of the Cutting Forces in End Milling," CIRP Ann., **28**(1), pp. 253–265.

[13] Winter, D. A., 1990, *Biomechanics and Motor Control of Human Movement*, Wiley, New York.

[14] Hitz, T., 1999, "The Digitally Sampled System: How Fast Is Fast Enough," http://www.sensorsmag.com/articles/0299/0299_da/index.htm, pp. 1–9.